DR. DILETTA OVERI (Orcid ID : 0000-0003-3561-8903)

DR. GUIDO CARPINO (Orcid ID : 0000-0001-8570-2519)

Article type : Original Article

Persistent Biliary Hypoxia and Lack of Regeneration Are Key Mechanisms in the Pathogenesis of Post-transplant Non-anastomotic Strictures

Iris E.M. de Jong[1,2] *, Diletta Overi[3] *, Guido Carpino[4], Annette S.H. Gouw[5], Marius C. van den Heuvel[5], Léon C. van Kempen[5], Carmine Mancone[6], Paolo Onori[3], Vincenzo Cardinale[7], Luca Casadei[8], Domenico Alvaro[9], Robert J. Porte[2] **, Eugenio Gaudio[3] **

*) share first authorship

**) share senior authorship

Affiliations: [1]Surgical Research Laboratory, Department of Surgery, University of Groningen, University Medical Center Groningen, Groningen, the Netherlands, [2]Section of Hepatobiliary Surgery and Liver Transplantation, Department of Surgery, University of Groningen, University Medical Center Groningen, Groningen, the Netherlands, [3]Department of Anatomical, Histological, Forensic Medicine and Orthopedic sciences, Sapienza University of Rome, Rome, Italy, [4]Division of Health Sciences, Department of Movement, Human and Health Sciences, University of Rome "Foro Italico", Rome, Italy, [5]Department of Pathology, University of Groningen, University Medical Center Groningen, Groningen, The Netherlands, [6]Department of Molecular Medicine, Proteomics Laboratory, Sapienza University of Rome, Rome, Italy, [7]Department of Medico-Surgical Sciences

This article has been accepted for publication and undergone full peer review but has not been through the copyediting, typesetting, pagination and proofreading process, which may lead to differences between this version and the Version of Record. Please cite this article as doi: 10.1002/HEP.32166

and Biotechnologies, Polo Pontino, Sapienza University of Rome, Rome, Italy, [8]Department of Chemistry, Sapienza University of Rome, Rome, Italy, [9]Department of Medicine and Medical Specialties, Sapienza University of Rome, Rome, Italy.

Key words: Orthotopic liver transplantation, post-transplant cholangiopathy, peribiliary glands, peribiliary vascular plexus, biliary complications
Financial support statement: This research was funded by research project grants from Sapienza University of Rome (EG, PO, DA).
Conflict of interest statement: the authors of this study have no conflict of interest to declare.
Title character count: 120

Main text word count (incl references): 6.548

Number of figures and tables: 8

Authors contributions: RJP had the initial conception for the study. **IEMdJ** and **DO** contributed by performing experiments and image analyses. Both were involved in the data interpretation**. GC** contributed to the design of the study, oversaw all the experiments, contributed to the image analyses and data interpretation. **VC** and **LC** contributed to the manuscript with the exo-metabolomics of isolated human BTSCs. **CM** contributed with the experiments. **ASHG** and **MvdH** performed the pathological evaluation of H&E stains. **LCvK** performed the qPCR experiments. The first drafts of the manuscript were written by **IEMdJ, RJP** and **GC.** Funding derived from grants obtained by **EG**, **DA** and **PO.** All authors reviewed the manuscript and edited the text.
Address for correspondence: Robert J Porte, MD, PhD**,** Section of Hepatobiliary Surgery and Liver Transplantation**,** Department of Surgery**,** University Medical Center Groningen**,** P.O. Box 30.001**,** 9700 RB Groningen**,** the Netherlands**.** Telephone: +31-50-3612896**.** Fax: +31-50-3614873**.** E-mail: r.j.porte@umcg.nl

List of abbreviations
αSMA: alpha smooth muscle actin

BTSC: biliary tree stem cell

CholM: cholangiocyte medium

CK7: cytokeratin 7

DBD: donation after brain death

DCD: donation after circulatory death

DR: ductular reaction

HAT: hepatic artery thrombosis

Hep-Par1: hepatocyte specific antigen

HIF-1α: hypoxia-inducible factor 1 alpha

KM: Kubota's Medium

MVD: microvascular density

NAS: non-anastomotic strictures

NCAM: neural cell adhesion molecule

NMR: nuclear magnetic resonance

OLT: orthotopic liver transplantation

PAS: periodic acid Schiff

PBG: peribiliary gland

PCNA: proliferating cell nuclear antigen

PHD2: prolyl hydroxylase domain-containing protein 2

PVP: peribiliary vascular plexus

SCTR: secretin receptor

SR/FG: sirius red/fast green

SQ: semi quantitative

Thy-1: Thymus cell surface antigen 1

VEGF-R2: VEGF receptor 2

VWF: von Willebrand factor

ABSTRACT

Background & Aims: Non-anastomotic biliary strictures (NAS) are a major cause of morbidity after orthotopic liver transplantation (OLT). Although ischemic injury of peribiliary glands (PBGs) and peribiliary vascular plexus (PVP) during OLT has been associated with the later development of NAS, the exact underlying mechanisms remain unclear. We hypothesized that bile ducts of patients with NAS suffer from ongoing biliary hypoxia and lack of regeneration from PBG stem/progenitor cells.

Approach & Results: Forty-two patients, requiring retransplantation for either NAS (n=18), hepatic artery thrombosis (HAT; n=13) or non-biliary graft failure (controls; n=11), were included in this study. Histomorphologic analysis of perihilar bile ducts was performed to assess differences in markers of cell proliferation and differentiation in PBGs, microvascular density, and hypoxia. In addition, isolated human biliary tree stem cells (hBTSCs) were used to examine exo-metabolomics during *in vitro* differentiation toward mature cholangiocytes.

Bile ducts of patients with NAS or HAT had significantly reduced indices of PBG mass, cellular proliferation and differentiation (mucus production, secretin receptor expression, primary cilia), reduced microvascular density, and increased PBG apoptosis and hypoxia marker expression, compared to controls. Metabolomics of hBTSCs during *in vitro* differentiation toward cholangiocytes revealed a switch from a glycolytic to oxidative metabolism, indicating the need for oxygen.

Conclusions: NAS are characterized by a microscopic phenotype of chronic biliary hypoxia due to loss of microvasculature, resulting in reduced proliferation and differentiation of PBG stem/progenitor cells into mature cholangiocytes. These findings suggest that persistent biliary hypoxia is a key mechanism underlying the development of NAS after OLT.

Biliary complications remain a major cause of morbidity and graft loss after orthotopic liver transplantation (OLT)(1). These complications are collectively identified as post-transplant cholangiopathy, and they may vary from anastomotic strictures and bile leakage to non-anastomotic biliary strictures (NAS), or even bile duct necrosis and intrahepatic biloma formation(2). NAS are generally defined as irregularities and strictures of the large intrahepatic and extrahepatic donor bile ducts, leading to recurrent cholestasis and/or cholangitis, in the presence of a patent hepatic artery (2,3). OLT recipients who develop NAS may have had an apparently uncomplicated transplant procedure, but typically present themselves with recurrent cholestasis and/or cholangitis at a median of 3-4 months postoperatively(4). The diagnosis of NAS is generally made on imaging of the biliary tree (i.e. endoscopic cholangiography or magnetic resonance cholangiography). Although biliary injury due to ischemia and/or bile salt toxicity during the transplant process has been associated with the occurrence of NAS(5,6), the exact pathogenesis underlying its development remains unclear. The nourishment of the biliary tree depends on the peribiliary vascular plexus (PVP) that derives from the hepatic artery(7,8). Hepatic artery thrombosis after OLT frequently leads to the formation of biliary strictures, but in the case of NAS the hepatic artery is shown to be patent(2).

The regeneration of large intrahepatic and extrahepatic bile ducts is supported by peribiliary glands (PBGs)(9). PBGs are sero-mucous glands which harbor a niche of stem/progenitor cells, the so-called biliary tree stem/progenitor cells (BTSCs)(10,11). These cells are characterized by high self-replication capabilities and the capacity to regenerate cholangiocytes and to restore damaged biliary surface epithelium(9,12,13). However, in pathological conditions, PBGs may be severely compromised and unable to exert their regenerative function(9,14). It has been suggested that insufficient regeneration due to loss of PBGs and/or microvascular damage may explain the development of NAS after OLT(6). Although bile duct injury at the time of OLT has been linked with the development of NAS, there are no studies that have examined the histopathological phenotype of end-stage NAS. We hypothesized that bile ducts with NAS suffer from ongoing (microscopic) biliary hypoxia and lack of regeneration from PBG stem/progenitor cells, despite a patent hepatic artery. To test this hypothesis, we performed a histomorphologic analysis of organs requiring retransplantation for NAS, hepatic artery thrombosis (HAT), or non-biliary causes of graft failure (controls). In this analysis, we focused on: 1) pathological changes with an emphasis on the PVP and PBGs; 2) epithelial regeneration; 3) fibrotic changes; and 4) the activation of ischemia-related pathways.

MATERIALS AND METHODS

Patients

A total of 42 adult OLT recipients, who required retransplantation of the liver at the University Medical Center Groningen (UMCG) between 1990 and 2016, were included in this study. Patients with primary sclerosing cholangitis were excluded. Eighteen patients required retransplantation for NAS within one year from the first OLT (NAS group), 13 were retransplanted for HAT (HAT group), and 11 patients required a retransplant for non-biliary causes, such as recurrence of viral or auto-immune hepatitis (controls).

In patients with NAS, imaging of the biliary tree was indicated based on clinical symptoms (i.e. fever, chills, jaundice), in combination with laboratory values indicating biliary pathology. NAS was diagnosed by endoscopic retrograde cholangio-pancreatography, magnetic resonance cholangio-pancreatography, or percutaneous transhepatic cholangiography, and defined as strictures, dilatations, or irregularities of the intra- or extrahepatic donor bile ducts in the absence of HAT. HAT was excluded by Doppler ultrasound. Isolated strictures at the bile duct anastomosis were excluded. Radiological locations of NAS in the biliary tree were classified as described by Buis, et al.(4). Early HAT was defined as absence of hepatic artery flow on Doppler ultrasound or computer tomography within 40 days after OLT, and always confirmed during the retransplant procedure.

Light microscopy, immunohistochemistry and immunofluorescence

Formalin-fixed, paraffin-embedded sections of explanted donor bile ducts and livers were obtained from the Pathology Department of the UMCG. All samples were taken from the hilar region of the explanted liver and included cross-sectional representations of the extrahepatic ducts as well as large intrahepatic bile ducts, with or without surrounding tissues. Three to four µm sections were prepared and stained with hematoxylin and eosin, periodic acid Schiff (PAS), Sirius red/fast green (SR/FG) and Masson's trichrome stain, according to standard protocols(15). The degree of necrosis, inflammation and fibrosis was assessed in routine stains.

For immunohistochemistry, endogenous peroxidase activity was blocked by a 30-min incubation in methanolic hydrogen peroxide (2.5%). Antigens were retrieved by applying Proteinase K (Dako, code S3020; Glostrup, Denmark) for 10 minutes at room temperature. Sections were then incubated overnight at 4°C with primary antibodies (**Supplementary Table 1**). Sections were incubated with secondary biotinylated antibody and then with Streptavidin-HRP (LSAB+ System-HRP, Dako, code K0690). Diaminobenzidine (Dako, code K3468) was used as substrate; sections were counterstained with hematoxylin.

To assess apoptosis, TUNEL assay (ApopTag® Peroxidase In Situ Apoptosis Detection Kit; Merck Millipore, Burlington, MA, USA) was performed according to manufacturer's protocol.

For immunofluorescence, non-specific protein binding was blocked by 5% normal goat serum. Specimens were incubated with primary antibodies, incubated for 1h with labelled isotype-specific secondary antibodies (AlexaFluor®, Invitrogen, Life Technologies Ltd, Paisley, UK), and finally, counterstained with DAPI for visualization of cell nuclei. Adequate negative controls were included for all immunostainings.

Slides were examined in a coded fashion using a Leica Microsystems DM4500B Light and Fluorescence Microscope (Weltzlar, Germany) and were scanned by a digital scanner (Aperio Scanscope CS/FL System, Aperio Digital Pathology, Leica Biosystems, Milan, Italy) and processed by ImageScope.

Ductular reaction (DR) in liver sections and the area occupied by PBGs (PBG mass) in bile ducts were evaluated in cytokeratin 7 (CK7)-stained sections and expressed as the percentage of the total analysis area(13). The number of destroyed PBG acini was counted as a percentage of the total number of acini; this percentage was converted in a semi-quantitative (SQ) score (0=<1%; 1=1–10%; 2=10–30%; 3=30–50%; 4=>50%). Microvascular density (MVD) was calculated as the area occupied by von Willebrand factor (vWF)+ and CD31+ vessels. Moreover, vessels were counted and expressed as number of vessels per microscopic field at 20x. Wall thickness was measured on SR-stained slides; the amount of SR+ fibers within the bile duct wall was quantified by a computer algorithm and expressed as area percentage. The number of CD68+ macrophages and α-smooth muscle actin (αSMA)+ cells was counted and expressed as number of cells per microscopic field at 40x. The number of positive cells in PBGs was automatically calculated by a computer algorithm; nuclear positivity was expressed as percentage of positive cells; for cytoplasmic stains, the previously mentioned SQ score was applied. The number of cells displaying a primary cilium was evaluated on α-acetylated tubulin-stained slides, and then expressed as SQ score.

Quantitative PCR analysis

Representative tissue samples of NAS (n=3), HAS (n=3) and control patients (n=2) were selected for gene expression analysis. Regions of interest indicated by a pathologist (MCvdH) were macrodissected from four 10μm FFPE sections. Subsequently, total RNA was isolated using

Qiagen's RNeasy FFPE kit (Qiagen, Germany) according to supplier's instruction and quantified using a Qubit Fluorometer (Invitrogen, ThermoFisher Scientific). cDNA was generated with Superscript II (Invitrogen), random hexamer primers (Invitrogen) and 500 µg total RNA input according to supplier's protocol. Per PCR reaction 2.5 µL of 4x diluted cDNA was used in a TaqMan Gene expression assay (Applied Biosystems, ThermoFisher) with fluorescently labelled primers (ThermoFisher, **Supplementary Table 2**) in a total volume of 10 µl. The Pfaffl method was used to calculate expression of the gene of interest relative to the expression of *PPIA* while accounting for differences in primer efficiencies(16).

Exo-metabolomics of Isolated Human BTSCs

Human BTSCs were isolated from extrahepatic biliary tree and cultured in a self-replication medium (i.e. Kubota's Medium: KM), as previously described(17)(18). For differentiation studies, cells were transferred in a medium for cholangiocyte differentiation (CholM) prepared by supplementing KM with calcium (final concentration: 0.6 mM), copper (10^{-12} M), 20 ng/ml bFGF, 20 ng/ml VEGF165, and 10 ng/ml HGF(18). One ml of culture medium was freeze dried for 24h. The resulting powder was dissolved in 600ml of phosphate D2O buffer solution pH 7.4, 3-(Trimethylsilyl)propionic-2,2,3,3-d4 acid sodium 1mM, and NaN_3 10mM. For the analysis of medium samples, the ^{1}H nuclear magnetic resonance (NMR) spectra were acquired on a Varian VNMRS 500 spectrometer at the frequency of 500MHz using a 2D *J*-resolved pulse sequence(19). After processing the NMR data, principal component analysis was performed using SIMCA-P+ v.12 (Umetrics, Umeå, Sweden).

Ethical Statement

Clinical data of donors and recipients were collected from the local transplant databases and individual electronic patient files. All tissue specimens were anonymously coded. Anonymized analysis of data and biomaterials was allowed as part of the TransplantLines cohort study (NCT03272841)(20). Protocols conformed to the ethical guidelines of the 1975 Declaration of Helsinki and were approved by the local Institutional Review Boards (Sapienza University of Rome, Rome, Italy(21-22) and METc UMCG 2017/638, registration number: 202000462, UMCG, Groningen, the Netherlands). No donor organs were obtained from executed prisoners or other institutionalized persons.

Statistical Analysis

Continuous data are presented as mean ± SD or as median and interquartile range (IQR). A One-way ANOVA test was used to calculate differences between the three groups. When a difference was identified by the One-way ANOVA test, a Bonferroni post-hoc test was applied to calculate the p-value. The Pearson correlation coefficient or the Spearman non-parametric correlation were used to determine the relationship between two variables. A p-value <0.05 was considered statistically significant. Analyses were performed using IBM SPSS software (IBM, Armonk, USA).

RESULTS

Donor and Recipient Characteristics

Clinical, biochemical, and surgical characteristics of donors and patients requiring retransplantation for non-biliary indications (controls), NAS or HAT are presented in **Table 1**. Indications for retransplantation in the control group are summarized in **Supplementary Table 3**. There were no significant differences in donor characteristics among the three groups, apart from a higher proportion of livers donated after circulatory death in the NAS group. NAS was diagnosed at a median of 82 (40-124) days after the first OLT. The time interval between the diagnosis of NAS and the retransplantation was 280 (109-2042) days. As expected, the time interval between the first and second OLT varied between the three groups. In the control group, livers were retransplanted at median of 1512 (854-3040) days after the initial OLT, whereas this time interval was 386 (143-2293) days in the NAS group and 7 (5-31) days in the HAT group. Serum values of liver function tests also differed among the three groups, as could be expected based on the underlying pathology.

Clinical and radiological characteristics of the patients undergoing retransplantation for NAS are summarized in **Table 2** and **Figure 1A**. All patients with NAS had strictures in zone A or B of the biliary tree, defined as the extrahepatic common bile duct and the extrahepatic part of the hepatic ducts, and the area between the intrahepatic hepatic ducts and second order branches (i.e. segmental intrahepatic bile ducts), respectively(4). Smaller biliary branches (i.e. area and septal intrahepatic bile ducts), more proximal from these levels (zone C and D), were generally not affected. Prior to retransplantation, most of the patients with NAS had undergone multiple interventions such as endoscopic retrograde cholangio-pancreatography and percutaneous transhepatic cholangiography drainage. Moreover, most patients who suffered from NAS presented with one or more episodes of cholangitis.

Liver Histopathology in Controls, NAS and HAT

Histologically, liver parenchyma in all samples was characterized by a variable degree of necrosis, inflammation, and fibrosis (**Supplementary Table 4** and **Supplementary Figure 1**). Liver parenchymal necrosis (F=0.372; p=0.695) and inflammation (F=0.803; p=0.464) did not differ between examined groups (i.e. Control, HAT, and NAS). Livers transplanted for non-biliary graft failure presented with bridging fibrosis or established cirrhosis in the parenchyma. However, the histology of large intra-hepatic bile ducts and hepatic ducts of these patients showed similarities with healthy ducts obtained from patients without liver or biliary diseases (see data in **Supplementary Figure 2**).

HAT livers showed less fibrosis (1±0.9) compared to the NAS (2.1±0.4; p=0.035) and control group (3.8±0.4; p<0.001), with the latter presenting the highest value (p<0.001 versus NAS). Finally, the extent of DR was lower in HAT (0.7±0.5%) and NAS (1.2±0.6%) livers compared to controls (3.5±1.9%; p=0.002 and p=0.008, respectively), whereas DR did not significantly differ between the NAS and HAT livers. DR significantly correlated with liver fibrosis (r=0.660; p=0.003).

Bile Duct Histopathology in Controls, NAS and HAT

Hematoxylin and eosin stains of bile ducts in the three groups revealed morphological differences. Bile ducts of control livers showed an intact surface epithelium and compact PBG clusters. Histological specimens derived from patients in the NAS group were heterogeneous but were generally characterized by a loss of surface biliary epithelium and destruction of the PBGs. The pretransplant number of episodes of cholangitis (**Table 2**) did not affect the histological score in the NAS group. The HAT group was characterized by loss of surface epithelial cells, detachment of PBG cells from their basement membrane, and the presence of microthrombi in the PVP, as well as intramural bleeding in some specimens (**Figure 1B**). The NAS group was characterized by higher degree of inflammation, compared to controls (p=0.023). Moreover, the NAS and HAT groups (8.9±4.6 and 9.7±2.9, respectively; **Supplementary Table 5**) showed a higher number of macrophages infiltrated in the duct wall compared to the control group (0.3±0.05, p<0.05; **Figure 1B/C**).

PBG Damage in NAS and HAT

The PBGs in NAS and HAT groups showed signs of severe injury (i.e. PBG dilatation and disruption). The PBG mass was significantly lower in NAS (1.7±0.8%) and HAT (1.9±1.4%) groups, compared to controls (4.3±1.9; p=0.039 and p=0.029, respectively) (**Figure 1B/C**). In accordance with this, the count of disrupted glands in the NAS (score: 2.4±1.2) and HAT (score: 2.5±0.9) groups were significantly higher, compared to controls (score: 0.5±0.6; p=0.021 and

p=0.013, respectively) (**Figure 1B/C**). No significant differences in PBG mass or injury were found between NAS and HAT groups. In NAS samples, no significant differences were found among patients that received a DCD (donation after circulatory death) versus DBD (donation after brain death) organ during the first OLT.

Histological specimens, taken from the peri-hilar region, included hepatic ducts and segmental bile ducts, as well as liver parenchyma where area, septal, and interlobular bile ducts were present. In the NAS group, when included in the section, area intrahepatic bile ducts did not display significant histological injury (**Supplementary Figure 3**). This enabled us to compare the histology of affected and non-affected bile ducts in patients with NAS. NAS-affected ducts were characterized by a lower PBG mass (1.6±0.8%) and a higher percentage of destroyed PBGs (score: 2.9±1.3), compared to non-affected ducts (6.9±4.0% and score: 0.5±0.5; p<0.001; **Supplementary Figure 3**). PBG mass and the percentage destroyed PBGs of non-affected ducts in patients with NAS did not differ from bile ducts in the control group. Therefore, in the following analyses, data were obtained from NAS-affected ducts.

PBG Proliferation, Apoptosis, and Senescence in NAS and HAT

Proliferation index of PBG cells was assessed by double immunostaining of PCNA and pan-cytokeratin (**Figure 2A/C**). In parallel with differences in PBG mass, the proliferation index was significantly lower in ducts with NAS (19.9±7.8%) or HAT (23.5±7.0%), compared to controls (40.5±17.9%; p=0.012 and p=0.042, respectively). Differences found in PBG mass and PCNA expression on a protein level were confirmed on an RNA level by quantitative PCR (**Supplementary Figure 4A/B**). No significant differences were found between the NAS and HAT groups. Notably, PBG proliferation index correlated significantly with total PBG mass (r=0.666 p=0.003).

PBG apoptosis was evaluated by IHC for cleaved caspase 3 and by TUNEL Assay (**Figure 2B/C**). PBG expression of cleaved caspase 3 was significantly higher in samples obtained from bile ducts from patients with NAS (score: 1.8±0.6) or HAT (score: 1.9±0.9), compared to controls (score: 0.6±0.5; p=0.031 and p=0.019, respectively). In parallel, TUNEL assay confirmed a higher percentage of apoptotic PBG cells in NAS (47.9±12.0%) or HAT (53.9±4.8%), compared to controls (10.1±6.8%; p<0.001 and p<0.001, respectively), without significant differences between the NAS and HAT groups. Finally, when cellular senescence was evaluated by IHC for γH2A.x, no significant differences were found between groups (**Figure 2B/C**). Additional immunostainings

for senescence markers p16 and p21 confirmed that there were no notable differences between the groups (**Supplementary Figure 5**).

PBG phenotype in NAS and HAT

Sox9 was used as a stem/progenitor cell marker within PBGs (**Figure 3A/F**); Sox9 positivity was significantly lower in the NAS (11.7±11.8%) and HAT (16.7±17.1%) groups, compared to controls (42.6±12.6%; p=0.010 and p=0.034, respectively). A significant correlation was found between the percentage of Sox9+ cells and the percentage of PCNA+ cells within PBGs (r=0.772; p<0.001). The number of PAS+ mucous PBG cells (**Figure 3B** and **3F**), was lower in NAS-affected (score: 1.4±1.0) and the HAT-affected ducts (score: 1.3±1.0) compared to controls (score: 3.0±1.4; p=0.045 and p=0.031, respectively). To evaluate the commissioning of PBG cells toward a mature cholangiocyte fate, secretin receptor (SCTR) expression and the presence of primary cilia were investigated (**Figure 3C/D/F**). SCTR expression was lower in the NAS (score: 1.5±0.5) and HAT (score: 0.8±0.6) groups, compared to the control group (score: 2.7±1.2; p=0.047 and p=0.002, respectively) which was corroborated by relative SCTR RNA expression (**Supplementary Figure 4C**). To examine the presence of primary cilia in PBG cells, we performed IF staining for α-acetylated tubulin as a marker of primary cilia (**Figure 3D/F**). The number of cells displaying a primary cilium was extremely reduced in ducts with NAS (score: 0.9±0.8) or HAT (score: 0.6±0.8), compared to controls (score: 2.5±1.3; p=0.014 and p=0.009, respectively), while there was no difference between the NAS and HAT groups. Interestingly, in histological specimens from patients with NAS, non-affected ducts were characterized by a similar percentage of PAS+ (score: 2.5±1.5) and SCTR+ (score: 2.5±0.5) cells within their PBGs as in controls (not shown).

Since PBG cells in the NAS and HAT groups appeared to express less mature cholangiocyte traits, we explored the possibility that PBGs would be committed to a hepatocyte fate (**Figure 3E**); however, the hepatocyte marker Hep-Par1 was negative in PBG cells in all examined samples.

Increased Collagen Deposition and Myofibroblast Activation in NAS

To evaluate fibrosis in the bile duct wall we analyzed SR/FG-stained and Masson's trichrome-stained sections (**Figure 4A/B; Supplementary Figure 6**). The average bile duct wall thickness appeared greater in patients with NAS (505±130μm), compared to the HAT group (184±63μm; p=0.002) or controls (172±68μm; p=0.002). No differences were found between HAT and controls. More specifically, when collagen fibers were evaluated, the extent of SR+ fibers within

the bile duct wall was higher in NAS (82.6±2.9%) compared to HAT (75.0±2.8%; p=0.03) or control specimens (76.8±2.4%; p=0.03). No differences were found between HAT and controls. Duct wall fibrosis was inversely correlated with PBG mass (r= -0.519, p<0.05).

Next, αSMA staining was used to evaluate myofibroblast activation in the bile duct wall and around PBGs (**Figure 4A/B** and **Supplementary Figure 7**). The area occupied by αSMA positive cells around PBGs was significantly higher in the NAS group (0.16±0.05 $\mu m^2/mm^2$), but not in the HAT group (0.09±0.11 $\mu m^2/mm^2$), compared to controls (0.04±0.01 $\mu m^2/mm^2$; p< 0.05). Interestingly, in the NAS group, a concentric organization of myofibroblasts was observed around the PBGs. Moreover, in NAS patients, non-affected ducts were characterized by a lower extent of αSMA+ cells around PBGs (0.07±0.012 $\mu m^2/mm^2$), compared to NAS-affected ducts (0.16±0.06 $\mu m^2/mm^2$; p<0.05).

To further characterize the activated myofibroblast population responsible for bile duct fibrosis in NAS, we performed stains in serial sections and immunofluorescence for Thy-1 (a specific marker for myofibroblasts) and NCAM (a specific marker for hepatic stellate cells). Our analysis demonstrated that fibrogenetic cells in ducts affected by NAS were Thy-1+/NCAM-, indicating that the main contributors to the fibrotic process in NAS-affected ducts are (myo-)fibroblasts within the bile duct wall (**Figure 4C** and **Supplementary Figure 8**). Finally, we investigated potential expression of pro-fibrogenetic factors by PBGs which could activate myofibroblasts (**Figure 4D and Supplementary Figure 9**), such as TGFβ1 and Sonic Hedgehog. In NAS and HAT, PBGs expressed higher levels of these factors (NAS: 2.4±0.5 and 2.20±0.4; HAT: 1.4±0.6; 1.80±0.5) compared to controls (0.4±0.6; 0.20±0.5; p<0.05)*.*

PVP Injury and Upregulation of Pro-angiogenic/Hypoxia Markers in NAS and HAT

The extension of the peribiliary vascular plexus and its modifications were studied by using the endothelial cell marker vWF (**Figure 5A/D**). The number of micro-vessels (per microscopic field at 20x) within the entire bile duct wall was significantly lower in the NAS (17.3±3.0) and HAT (11.2±2.6) groups, compared to controls (25.4±1.4; p<0.001 and p<0.001, respectively). Moreover, the microvascular density (MVD) around PBGs was significantly reduced in the NAS (0.0044±0.0017 $\mu m^2/mm^2$) and HAT (0.005±0.001 $\mu m^2/mm^2$) groups, compared to controls (0.015±0.008 $\mu m^2/mm^2$; p=0.038 and p=0.008, respectively). Moreover, quantitative PCR revealed that vWF expression on an RNA level was significantly lower in the NAS and HAT groups, with HAT showing the lowest expression (**Supplementary Figure 10A**). These findings were confirmed by immunohistochemistry for CD31 (**Supplementary Figure 11**). To further

characterize micro-vascular damage (**Figure 5B/C/D**), endothelial cell injury and apoptosis were evaluated. NAS and HAT showed higher degrees of endothelial cell injury (score in NAS: 1.6±0.6; score in HAT: 2.6±0.5) and a higher number of TUNEL+ apoptotic endothelial cells (score in NAS: 2.6±0.6; score in HAT: 2.0±1.0) compared to controls (score: 0.2±0.4 and 0.6±0.5; $p<0.05$). Moreover, HAT presented with higher endothelial cell injury compared to NAS ($p=0.030$), but no differences in endothelial cell apoptosis were found between these two groups.

We next examined the expression of key pathway elements in angiogenesis (i.e. VEGFs) and hypoxia (i.e. hypoxia inducible factor 1α – HIF-1α, and prolyl hydroxylase domain-containing protein 2 – PHD2) in the PBGs (**Figure 6A-C**). VEGF-A expression in PBGs was significantly higher in NAS-affected ducts (score: 2.3±1.0), but not in HAT ducts (score: 0.9±0.6), compared to controls (score: 0.7±0.8; $p=0.03$). This finding was supported by quantitative PCR, although not significant (**Supplementary Figure 10B**). VEGF-C expression was mostly negative in PBGs in all examined groups (**Figure 6A**). We next evaluated the expression of VEGF-R2, the main VEGF-A receptor (**Figure 6B**). Within the bile duct walls, this marker was mainly expressed in blood vessels; the number of VEGF-R2 positive vessels was significantly reduced in HAT (2.2±0.5) and NAS (4.3±0.8) compared to controls (8.5±0.4; $p<0.05$). Accordingly, relative VEGFR2 RNA expression was reduced in NAS and HAT samples compared to controls (**Supplementary Figure 10C).** HIF-1α expression (**Figure 6C**) was significantly higher in bile ducts of patients with NAS (score: 2.0±1.0) or HAT (score: 1.6±0.8), compared to controls (score: 0.7±0.8; $p=0.021$ and $p=0.045$, respectively), which was confirmed on an RNA level (**Supplementary Figure 10D**). Finally, the expression of PHD2 by PBG cells was significantly lower in NAS (score: 0.8±1.0) and HAT (score: 1.0±0.7) ducts compared to controls (score: 2.8±0.8; $p=0.012$ and $p= 0.024$, respectively) without significant differences between NAS and HAT groups.

Metabolome in Human BTSCs Differentiating into Mature Cholangiocytes

To evaluate whether stem cells modify their metabolism while differentiating into mature cholangiocytes, human BTSCs (n=5 biological replicates) were cultured in self-replicating conditions (i.e. KM) and then transferred into a medium tailored for cholangiocyte differentiation (CholM) for 14 days (**Figure 6D**). Culture media were collected after 14 days in KM (T1) and after 14 days in CholM (T2). Collected media were analyzed by NMR and explored by principal component analysis, producing a solution with two significant components, cumulatively explaining 85% of the total variance in the data (**Figure 6D**). From the analysis of loadings, a significant shift from a high to a low glycolytic phenotype was observed in human BTSCs in CholM compared to KM, as indicated by the negative correlation between glucose consumption

(factor loading=-0.73) and lactate production (factor loading=+0.83) loadings: glucose flux dropped off in CholM, leading to reduced lactate accumulation. The positive correlation pattern between glutamine consumption (factor loading=+0.80) and alanine (factor loading=+0.87) and lactate production loadings demonstrates a decrease in glutaminolysis flux, thus indicating a potential decreased flux through the alanine aminotransferase pathway to supply α-Ketoglutarate to the tricarboxylic acid cycle. **Figure 6D** reports metabolites with significant differences between T1 (KM) and T2 (CholM).

DISCUSSION

This study provides microscopic evidence that chronic local ischemia due to diminished bile duct microvasculature is a key mechanism underlying the pathogenesis of NAS after OLT. Due to the ongoing biliary hypoxia, the physiological regenerative process, originating from the BTSCs, residing in the PBGs, is compromised. While grafts suffering from NAS by definition have a patent hepatic artery, the microscopic biliary and vascular abnormalities observed in these bile ducts were very similar to those observed after HAT. Despite the dual blood supply of the liver via the portal vein and hepatic artery, bile ducts are known to be largely dependent on the hepatic artery for the delivery of oxygen and nutrients. The main histological difference between bile ducts suffering from NAS or HAT was a significantly increased deposition of collagen matrix and activation of myofibroblasts in the former group, resulting in increased bile duct wall thickness and fibrosis. These signs of fibrotic wall thickening were in line with the radiological presentation of NAS, which was characterized by irregularities and narrowing of the donor bile ducts.

This is the first study that provides a detailed microscopic analysis of the bile ducts of donor livers suffering from NAS. In previous studies of biopsies taken from donor bile ducts at the time of OLT, it was noted that almost all transplanted organs have a substantial amount of bile duct injury after cold ischemic preservation(6,23). This is characterized by loss of the surface epithelium, and a varying degree of injury of stroma cells, endothelium of the PVP and epithelial cells of the PBGs(6). Although these alterations are frequently observed in bile ducts at the time of OLT, the majority of these organs does not develop NAS and shows a complete regeneration of the bile duct wall, including PBG compartment, stroma and vessels as we observed in the control group included in this study. In contrast, cases that later developed NAS have been identified at the time of OLT by a more severe injury of the PVP and extramural PBGs(6). Since the PBGs are a niche of BTSCs from which surface biliary epithelium can regenerate after severe injury, it has been suggested that insufficient regeneration is a key event underlying the pathogenesis of

NAS(6,9,23,24). However, formal evidence that bile ducts from liver grafts with end-stage NAS display features of a persistent hypoxic condition and insufficient regeneration was never provided so far.

In the current study we aimed to describe the microscopic phenotype of bile ducts that developed severe NAS, requiring retransplantation of the liver. We hypothesized that these bile ducts would have evidence of ongoing hypoxia and lack of regeneration from PBG stem/progenitor cells. As positive and negative controls of hypoxia we used bile ducts from livers that required retransplantation for early HAT or non-biliary causes of graft failure, such as recurrent viral or auto-immune hepatitis. By using these control groups, we were able to demonstrate that the bile duct injury observed in NAS is indeed compatible with (ongoing) hypoxia after the OLT procedure, despite a patent hepatic artery. Bile ducts of livers that required retransplantation for non-biliary and non-ischemic causes of graft failure had normal microscopic architecture, characterized by intact surface epithelium and healthy appearing PVP and PBGs. Biliary epithelial cells in these ducts appeared to be successfully regenerated and restored post-transplantation. In contrast to this, bile ducts with NAS or HAT had evidence of a diminished microvascular density, altered expression of hypoxia pathway elements (i.e. HIF-1α and its regulator PHD2)(25), reduced PBG mass, and increased PBG apoptosis. In parallel with this, we found evidence of reduced PBG stem/progenitor cell proliferation and diminished differentiation toward mature cells (mucus production, secretin receptor expression and presence of primary cilia) in bile ducts with NAS or HAT, compared to controls.

The only two differences between bile ducts affected by NAS and HAT were increased fibrosis and VEGF-A expression in the ducts with NAS, but not in those with HAT. Bile ducts with NAS displayed markedly increased deposition of collagen and myofibroblast activation, resulting in wall thickening. Our data suggest that hypoxic damage of the PBGs could trigger the expression of pro-fibrogenetic factors, such as TGFβ1 and Sonic Hedgehog, which can activate myofibroblasts in a paracrine fashion. Differences in bile duct wall fibrosis between NAS and HAT could be explained by the longer time interval between the first transplant and retransplantation in the NAS group, compared to the HAT group. We intentionally selected only bile ducts with early HAT (<40 days) since HAT occurring at a longer time interval after OLT does not always lead to clinically overt bile duct ischemia as arterial collaterals may have been developed in this situation(26). Therefore, in contrast to early HAT, late HAT frequently does not require retransplantation(27).

The microscopic picture of bile duct wall fibrosis and thickening matched the one of radiological imaging, which was characterized by irregularities and narrowing of the donor bile ducts. As described previously, NAS typically affects the extrahepatic common bile duct, hepatic ducts and the segmental intrahepatic donor bile ducts, whereas smaller intrahepatic branches are usually spared(4). In accordance with the radiological presentation of NAS, we identified relatively well preserved and healthy appearing area, septal and interlobular bile duct branches in the same sections as the affected bile ducts. PBGs in the non-affected branches were not histomorphologically different from those in control bile ducts. These findings confirm that post-transplant NAS mainly occurs in the extrahepatic common bile duct, hepatic ducts and the segmental intrahepatic donor bile ducts. Of note, previous work demonstrated that DCD organs are more prone to develop NAS and show increased damage of the PBGs during the transplant procedure(28). In our cases, no significant differences were found among NAS patients when comparing bile duct samples of patients that received a DBD vs DCD organ. Therefore, the number of DCD organs in the NAS group did not influence our analysis. However, further studies on a larger population will be needed to thoroughly assess the presence of specific characteristics of NAS in DCD vs DBD donors.

The difference in VEGF-A expression in PBGs of bile ducts with NAS or HAT is remarkable. Both bile ducts affected by NAS or HAT displayed increased PBG expression of HIF-1α, but VEGF-A expression was only increased in NAS. A possible explanation for this is the presence of chronic (ongoing) biliary hypoxia in bile ducts that develop NAS, compared to the more acute hypoxia after HAT(4,26). Increased VEGF-A expression in PBG cells of bile ducts with NAS could represent a compensative response to overcome the prolonged biliary hypoxia(29). Residual PBGs both in HAT- and NAS-affected ducts showed negligible signs of mature cholangiocyte commitment. In line with this, our *in vitro* study using isolated human BTSCs demonstrated that the metabolomic profile of BTSCs shifts from a glycolytic metabolism in self-replication conditions to an oxidative one as differentiation to mature cholangiocytes takes place. The basal glycolytic metabolism in human BTSCs within PBGs could explain their relative resistance to ischemia-reperfusion injury during the transplant procedure, compared to cholangiocytes lining the surface epithelium(30,31). Interestingly, human BTSC differentiation into mature cholangiocytes was associated with the inhibition of glutaminolysis and the consumption of amino acids, likely for anabolic purposes. Thus, differentiation and anabolic reconstruction –which are essential elements of regeneration– may be impeded in PBGs in NAS-affected ducts due to ongoing oxygen shortage (i.e. hypoxia)(32). Several studies in experimental models demonstrated that bile duct regeneration is supported by the preservation of the PVP and that hepatic artery ligation

impairs biliary epithelial cell proliferation(29). In line with this, our study further highlights the importance of the PVP in biliary regeneration. Insufficient and timely restoration of the bile duct microvasculature after OLT results in ongoing local hypoxia, leading to lack of biliary regeneration and subsequent fibrotic narrowing of the bile ducts. This implies that optimal preservation of the PVP should be a key target of liver graft preservation prior to OLT.

In an *ex vivo* model of human bile duct regeneration after cold ischemia-induced injury, using precision-cut bile duct slices, we previously demonstrated that BTSCs residing in the PBGs are able to respond to bile duct epithelial loss with proliferation, differentiation, and maturation to restore epithelial integrity(9). In accordance with the current *in vivo* findings, bile duct regeneration in the *ex vivo* model was accompanied by increased expression of HIF-1α and VEGF-A. Moreover, in the *ex vivo* model, regeneration was accompanied by myofibroblast activation and increased collagen deposition in the stroma in a concentric fashion around PBGs. These changes in bile duct matrix were also observed in the current clinical study and likely contributed to stricture formation.

A limitation of this study could reside in the lack of data from PBG cells directly isolated from diseased organs. A full molecular study of isolated cells would furnish further insights in the pathogenesis of this disease. However, such analysis could represent an obstacle for successive studies given the difficulties in tissue procurement and the presence of a fibrosis niche around PBGs in NAS-affected ducts which would make the isolation of viable cells difficult.

In conclusion, our findings suggest that persistent biliary hypoxia due to loss of microvasculature is a key mechanism underling the development of NAS after OLT. NAS-affected ducts are characterized by a histomorphological phenotype of chronic biliary hypoxia due to loss of microvasculature/PVP, resulting in reduced proliferation and differentiation of PBG stem/progenitor cells into mature cholangiocytes. The absence of a regenerative response is accompanied by increased fibrosis of bile duct wall, compatible with the radiological presentation of bile duct strictures. Optimal preservation of the PVP should, therefore, be a key target in donor organ preservation to avoid the development of NAS after OLT.

REFERENCES

(1) Kochhar G, Parungao JM, Hanouneh IA, Parsi MA. Biliary complications following liver transplantation. World J Gastroenterol 2013;19:2841-2846.

(2) **de Vries Y, von Meijenfeldt FA**, Porte RJ. Post-transplant cholangiopathy: Classification, pathogenesis, and preventive strategies. Biochim Biophys Acta Mol Basis Dis 2018;1864:1507-1515.

(3) Guichelaar MMJ, Benson JT, Malinchoc M, Krom RAF, Wiesner RH, Charlton MR. Risk factors for and clinical course of non-anastomotic biliary strictures after liver transplantation. Am J Transplant 2003;3:885-890.

(4) Buis CI, Verdonk RC, Van der Jagt, Eric J., van der Hilst, Christian S., Slooff MJH, Haagsma EB, et al. Nonanastomotic biliary strictures after liver transplantation, part 1: Radiological features and risk factors for early vs. late presentation. Liver Transpl 2007;13:708-718.

(5) Buis CI, Geuken E, Visser DS, Kuipers F, Haagsma EB, Verkade HJ, et al. Altered bile composition after liver transplantation is associated with the development of nonanastomotic biliary strictures. J Hepatol 2009;50:69-79.

(6) op den Dries S, Westerkamp AC, Karimian N, Gouw ASH, Bruinsma BG, Markmann JF, et al. Injury to peribiliary glands and vascular plexus before liver transplantation predicts formation of non-anastomotic biliary strictures. J Hepatol 2014;60:1172-1179.

(7) Gaudio E, Onori P, Pannarale L, Marinozzi G. Microcirculation of the extrahepatic biliary tree: a scanning electron microscopy study of corrosion casts. J Anat 1993:37-44.

(8) Castaing D. Surgical anatomy of the biliary tract. HPB (Oxford) 2008;10:72-76.

(9) **de Jong IEM, Matton APM,** van Praagh JB, van Haaften WT, Wiersema-Buist J, van Wijk LA, et al. Peribiliary Glands Are Key in Regeneration of the Human Biliary Epithelium After Severe Bile Duct Injury. Hepatology 2019;69:1719-1734.

(10) **Carpino G, Cardinale V**, Onori P, Franchitto A, Berloco PB, Rossi M, et al. Biliary tree stem/progenitor cells in glands of extrahepatic and intraheptic bile ducts: an anatomical in situ study yielding evidence of maturational lineages. J Anat 2012;220:186-199.

(11) **DiPaola F, Shivakumar P**, Pfister J, Walters S, Sabla G, Bezerra JA. Identification of intramural epithelial networks linked to peribiliary glands that express progenitor cell markers and proliferate after injury in mice. Hepatology 2013;58:1486-1496.

(12) Carnevale G, Carpino G, Cardinale V, Pisciotta A, Riccio M, Bertoni L, et al. Activation of Fas/FasL pathway and the role of c-FLIP in primary culture of human cholangiocarcinoma cells. Sci Rep 2017;7:14419.

(13) **Carpino G, Nevi L,** Overi D, Cardinale V, Lu W, Di Matteo S, et al. Peribiliary Gland Niche Participates in Biliary Tree Regeneration in Mouse and in Human Primary Sclerosing Cholangitis. Hepatology 2020;71:972-989.

(14) Carpino G, Cardinale V, Renzi A, Hov JR, Berloco PB, Rossi M, et al. Activation of biliary tree stem cells within peribiliary glands in primary sclerosing cholangitis. J Hepatol 2015;63:1220-1228.

(15) Carpino G, Cardinale V, Folseraas T, Overi D, Floreani A, Franchitto A, et al. Hepatic Stem/Progenitor Cell Activation Differs between Primary Sclerosing and Primary Biliary Cholangitis. Am J Pathol 2018;188:627-639.

(16) Pfaffl MW. A new mathematical model for relative quantitative in real-time RT-PCR. Nucleic Acids Res 2001;29:e45

(17) Costantini D, Overi D, Casadei L, Cardinale V, Nevi L, Carpino G, et al. Simulated microgravity promotes the formation of tridimensional cultures and stimulates pluripotency and a glycolytic metabolism in human hepatic and biliary tree stem/progenitor cells. Sci Rep 2019;9:5559.

(18) **Carpino G, Cardinale V**, Gentile R, Onori P, Semeraro R, Franchitto A, et al. Evidence for multipotent endodermal stem/progenitor cell populations in human gallbladder. J Hepatol 2014;60:1194-1202.

(19) Casadei L, Valerio M. (1)H NMR Metabolomic Footprinting Analysis for the In Vitro Screening of Potential Chemopreventive Agents. Methods Mol Biol 2016;1379:89-97.

(20) **Eisenga MF, Gomes-Neto AW**, van Londen M, Ziengs AL, Douwes RM, Stam SP, et al. Rationale and design of TransplantLines: a prospective cohort study and biobank of solid organ transplant recipients. BMJ Open 2018;8:e024502.

(21) Costantini D, Overi D, Casadei L, Cardinale V, Nevi L, Carpino G, et al. Simulated microgravity promotes the formation of tridimensional cultures and stimulates pluripotency and a glycolytic metabolism in human hepatic and biliary tree stem/progenitor cells. Sci Rep 2019;9:5559.

(22) Wang Y, Lanzoni G, Carpino G, Cui C, Dominguez-Bendala J, Wauthier E, et al. Biliary tree stem cells, precursors to pancreatic committed progenitors: evidence for possible life-long pancreatic organogenesis. Stem Cells 2013;31:1966-1979.

(23) Karimian N, Op den Dries S, Porte RJ. The origin of biliary strictures after liver transplantation: is it the amount of epithelial injury or insufficient regeneration that counts? J Hepatol 2013;58:1065-1067.

(24) Sutton ME, op den Dries S, Koster MH, Lisman T, Gouw ASH, Porte RJ. Regeneration of human extrahepatic biliary epithelium: the peribiliary glands as progenitor cell compartment. Liver Int 2012;32:554-559.

(25) Epstein AC, Gleadle JM, McNeill LA, Hewitson KS, O'Rourke J, Mole DR, et al. C. elegans EGL-9 and mammalian homologs define a family of dioxygenases that regulate HIF by prolyl hydroxylation. Cell 2001; 107:43-54.

(26) Frongillo F, Lirosi MC, Nure E, Inchingolo R, Bianco G, Silvestrini N, et al. Diagnosis and Management of Hepatic Artery Complications After Liver Transplantation. Transplant Proc 2015;47:2150-2155.

(27) Pareja E, Cortes M, Navarro R, Sanjuan F, López R, Mir J. Vascular complications after orthotopic liver transplantation: hepatic artery thrombosis. Transplant Proc 2010;42:2970-2972.

(28) Franchitto A, Overi D, Mancinelli R, Mitterhofer AP, Muiesan P, Tinti F, et al. Peribiliary gland damage due to liver transplantation involves peribiliary vascular plexus and vascular endothelial growth factor. Eru J Histochem 2019;63:3022.

(29) **Gaudio E, Barbaro B**, Alvaro D, Glaser S, Francis H, Franchitto A, et al. Administration of r-VEGF-A prevents hepatic artery ligation-induced bile duct damage in bile duct ligated rats. Am J Physiol Gastrointest Liver Physiol 2006;291:307.

(30) Fujiwara H, Tateishi K, Misumi K, Hayashi A, Igarashi K, Kato H, et al. Mutant IDH1 confers resistance to energy stress in normal biliary cells through PFKP-induced aerobic glycolysis and AMPK activation. Sci Rep 2019;9:18859.

(31) Ryall JG, Cliff T, Dalton S, Sartorelli V. Metabolic Reprogramming of Stem Cell Epigenetics. Cell Stem Cell 2015;17:651-662.

(32) Gaudio E, Franchitto A, Pannarale L, Carpino G, Alpini G, Francis H, et al. Cholangiocytes and blood supply. World J Gastroenterol 2006;12:3546-3552.

ACKNOWLEDGEMENT

We thank Mirjam Koster for her contribution on the p16 and p21 immunostainings.

FIGURE LEGENDS

Fig.1. Radiologic and microscopic presentation of non-anastomotic strictures (NAS). **(A)** Endoscopic retrograde cholangiography showing NAS at the level of the hepatic duct and segmental intrahepatic bile ducts (green area), around the hilar region. **(B)** Hematoxylin and eosin (H&E) stains (upper panels), and immunohistochemistry for CD68 (middle panels) and

cytokeratin 7 (CK7, lower panels) of bile duct specimens obtained from patients retransplanted for non-biliary causes (Control), non-anastomotic strictures (NAS), or for hepatic artery thrombosis (HAT). In comparison to controls, bile ducts affected by NAS and HAT were characterized by loss of surface epithelium (arrowheads) and stroma destruction (asterisk). Infiltrating CD68+ macrophages (arrows, middle panels) can be observed in NAS, and HAT. In the lower panels, arrows indicate damaged PBGs in NAS and HAT, magnified in the circles below. **(C)** Histograms show quantification (mean and SD) of CD68+ cells, destroyed PBGs, and PBG mass. *p<0.05 vs other groups.

Fig.2. Peribiliary gland (PBG) proliferation, apoptosis, and senescence.
(A) Immunofluorescence for pan-cytokeratin (pCK, green) and proliferating cell nuclear antigen (PCNA, red) of bile duct specimens obtained from patients retransplanted for non-biliary causes (Control), non-anastomotic strictures (NAS), or hepatic artery thrombosis (HAT). Nuclei are counterstained with DAPI and displayed in blue. **(B)** TUNEL assay (upper panels), and immunohistochemistry for cleaved (c)Caspase 3 (middle panels) and γH2A.x (lower panels). Arrows indicate positive cells. Scale bars: 100μm. **(C)** Histograms show quantification (mean and SD) for PCNA (PBG proliferation index) and TUNEL (PBG apoptosis) positive cells within PBGs, and for the semiquantitative score of cCaspase 3 (PBG apoptosis) and γH2A.x (PBG senescence). * p< 0.05 vs other groups.

Fig.3. Peribiliary gland (PBG) cell phenotype.
(A) Immunohistochemistry for transcription factor Sox9 in bile duct specimens obtained from patients retransplanted for non-biliary causes (Control), non-anastomotic strictures (NAS), or for hepatic artery thrombosis (HAT). Scale bars: 100μm. **(B)** Immunohistochemistry for cytokeratin 7 (CK7) counterstained with periodic acid Schiff (PAS) in control, NAS and HAT groups. Scale bars: 50μm. **(C)** Immunohistochemistry for secretin receptor (SCTR) in control, NAS, and HAT group. Scale bars: 50μm. **(D)** Double immunofluorescence for α-acetylated tubulin (αTub, green) and SCTR (red) in control, NAS, and HAT group. Green arrows indicate cells with primary cilium (PC). Original magnification: 40x. **(E)** Immunofluorescence for CK7 and hepatocyte-paraffin 1 (HepPar-1) in specimens of NAS-affected bile ducts. Original magnification: 10x. Asterisk indicates hepatocytes within liver parenchyma (positive control for HepPar1); PBGs are indicated by green arrows and magnified in the circle. **(F)** Heat map reports semi-quantitative (SQ) scores for Sox9, PAS and SCTR positivity, and for the cells with PC in PBGs. CTR: control. In A-C, arrows indicate positive cells within PBGs. In D-E, nuclei are counterstained with DAPI and displayed in blue.

Fig.4. Collagen fiber deposition and myofibroblast activation.
(A) Sirius red/fast green (SR/FG) stain (upper panels), Masson's trichrome stain (middle panels) and immunohistochemistry for α-smooth muscle actin (αSMA) in bile duct specimens obtained from patients retransplanted for non-biliary causes (Control), non-anastomotic strictures (NAS), or for hepatic artery thrombosis (HAT). In A, inset bars show the duct wall thickness. L: lumen. Scale bars: 500μm (SR/FG and Masson) and 50μm (αSMA). **(B)** Histograms show quantification (mean and SD) of duct wall thickness, collagen content of bile duct walls (expressed as percentage of bile duct wall) and of the number of αSMA+ cells per mm^2 area around PBGs. *p<0.05 vs other groups. **(C)** Immunohistochemistry on serial sections for Thymus cell surface antigen 1 (Thy-1) and Neural cell adhesion molecule (NCAM, upper panels) and double immunofluorescence (lower panels) for Thy-1 and αSMA (left) and for NCAM and Thy-1 (right) in NAS specimen. Scale bars: 100μm (upper panels) and 50μm (lower panels). **(D)** Double immunofluorescence for TGFβ1 (green, upper panels) and Sonic Hedgehog (SHH, green, lower panels) with cytokeratin 7 (CK7, red) of Control, NAS, and HAT groups. Original magnification: 40x. In C-D, nuclei are counterstained with
DAPI and displayed in blue.

Fig.5. Modifications of the peribiliary vascular plexus.
(A) Immunohistochemistry for von Willebrand Factor (vWF) in bile duct specimens obtained from patients retransplanted for non-biliary causes (Control), non-anastomotic strictures (NAS) or for hepatic artery thrombosis (HAT). vWF+ vessels (arrows) and the microvascular density (MVD) around PBGs (arrowheads) are shown. Areas in the circles are magnified below. Scale bars: 200μm. **(B)** Hematoxylin and eosin (H&E) stains show normal vessels (arrows) and damaged ones (arrowheads) in the bile duct wall. Areas in the squares are magnified below. Original magnification: 20x. **(C)** TUNEL assay shows non-apoptotic (blue arrows) and apoptotic (brown arrows) endothelial cells. Original magnification: 40x. **(D)** Histograms show quantification (mean and SD) of vWF+ microvessels (MV) density within bile ducts, score of endothelial cell (EC) disruption, and TUNEL+ endothelial cells. *p<0.05 vs other groups.

Fig. 6. Angiogenic response and metabolism of peribiliary gland (PBG) cells.
(A) Immunohistochemistry for vascular endothelial growth factor A (VEGF-A, upper panels) and vascular endothelial growth factor C (VEGF-C, lower panels) in bile duct specimens obtained from patients retransplanted for non-biliary causes (Control), non-anastomotic strictures (NAS) or for hepatic artery thrombosis (HAT). Heat map reports semi-quantitative (SQ) scores for VEGF-A

and VEGF-C positivity in peribiliary glands (PBGs). Scale bars: 100μm. **(B)** Immunohistochemistry for VEGF-R2. Original magnification: 40x. Histogram shows quantification (mean and SD) of VEGF-R2+ vessels per high power field (40x). *p<0.05 vs other groups. **(C)** Immunohistochemistry for hypoxia-inducible factor-1α (HIF-1α, upper panels) and for prolyl hydroxylase domain-containing protein 2 (PHD2, lower panels). Scale bars: 100μm. Heat map shows SQ scores for HIF-1α and PHD2 expression in PBGs. **(D)** Human biliary tree stem/progenitor cells (hBTSCs) were cultured in self-replicating conditions (Kubota's Medium: KM) for 14 days (T1) and then transferred in a medium tailored for cholangiocyte differentiation (CholM) for another 14 days (T2). Metabolites in collected media were analyzed by nuclear magnetic resonance and explored by principal component (PC) analysis, producing a solution with 2 significant components, cumulatively explaining 85% of the total variance in the data. The histogram shows quantification (means and SD) of metabolites in culture medium with significant differences comparing T1 with T2.

TABLES

Table 1. Clinical and Surgical Characteristics of Donors and Recipients

Variable	Control (n=11)	NAS (n=18)	HAT (n=13)	P-values
Donor characteristics				
Age (years)	50(45-53)	45(39-56)	53(49-59)	0.69
Gender - Male - Female	 2(20%) 8(80%)	 10(56%) 8(44%)	 5(42%) 7(58%)	0.20
GGT (U/L)	14(9-31)	20(17-59)	27(14-83)	0.25
Type of donor - DCD - DBD	 0 9(82%)	 7(39%) 11(61%)	 1(8%) 11(85%)	**0.03**[a]
Cold ischemia time (hr:min)	10:02(7:39-13:52)	8:34(7:21-10:37)	8:19(7:06-10:06)	0.22
Warm ischemia time (hr:min)	0:54(0:46-0:57)	0:51(0:39-1:02)	0:47(0:35-0:55)	0.31
Recipient characteristics				
Age (years)*	41(22-50)	47(35-56)	52(40-56)	0.13
Gender - Male - Female	 5(45%) 6(55%)	 7(39%) 11(61%)	 5(38%) 8(62%)	0.93
MELD score	20(15-23)	22(15-25)	19(12-23)	0.29
Days between first and second transplant	1512(854-3040)	386(143-2293)	7(5-31)	**0.01**[b]

Bile duct anastomosis at first OLT				
- Duct-to-duct	11(100%)	16(89%)	9(70%)	0.22
- Hepatico-jejunostomy	0	2(11%)	3(23%)	
Surgical technique				
- Classical	4(36%)	3(17%)	1(8%)	0.35
- Piggyback	6(55%)	15(83%)	12(92%)	
Laboratory serum values**				
AST (U/L)	55(30-148)	105(70-157)	366(90-2036)	0.07
ALT (U/L)	54(19-100)	69(54-117)	614(88-2262)	**0.00**[b,c]
GGT (U/L)	91(58-431)	344(202-734)	92(52-380)	0.30
ALP (U/L)	133(78-265)	484(205-756)	143(111-244)	0.24
Bilirubin (µmol/L)	53(15-607)	169(55-274)	49(20-111)	0.37
Albumin (g/L)	34(29-35)	34(29-38)	18(12-25)	**0.00**[b,c]

Data are expressed as median and interquartile range; p-values <0.05 are in bold. Abbreviations: HAT, hepatic artery thrombosis; NAS, non-anastomotic strictures; DCD, donors after cardiac death; DBD, donors after brain death; MELD, model for end-stage liver disease; ALP, alkaline phosphatase; AST, aspartate aminotransferase; ALT, alanine aminotransferase; GGT, gamma glutamyl transferase. In some groups, numbers do not add up due to missing data.

*) At time of first transplant

**) Prior to retransplantation

[a]) Post-hoc test showed a p<0.05 between Control and NAS group

[b]) Post-hoc test showed a p<0.05 between Control and HAT group

[c]) Post-hoc test showed a p<0.05 between NAS and HAT group

Variable	Number (%)

Table 2. Clinical and Radiological Characteristics of Patients in the NAS Group

Radiological localization of NAS*	
- Zone A	15(83%)
- Zone B	3(17%)
- Zone C	0
- Zone D	0
History of bile leakage	
- Yes	7(39%)
- No	11(61%)
Appearance of casts and/or sludge on ERCP/MCRP	
- Cast(s), sludge or both	6(33%)
- Not present or not described	12(67%)
Interventions prior to retransplant	
- None	1(6%)
- ERCP without balloon dilatation and stenting	2(11%)
- ERCP with balloon dilatation and/or stenting	4(22%)
- ERCP + PTCD	5(28%)
- Surgery	1(6%)
- ERCP + surgery	4(22%)
- PTCD + ERCP + surgery	1(6%)
Episodes of cholangitis	
- None	6(33%)
- 1-2	4(22%)
- Recurrent cholangitis (>2)	8(44%)

Data are expressed as numbers with percentage.

Abbreviations: NAS, non-anastomotic strictures; ERCP, endoscopic retrograde cholangiopancreatography; MRCP, magnetic resonance cholangiopancreatography; PTCD, percutaneous transhepatic cholangiodrainage.

*) Based on classification described by Buis et al.(4)

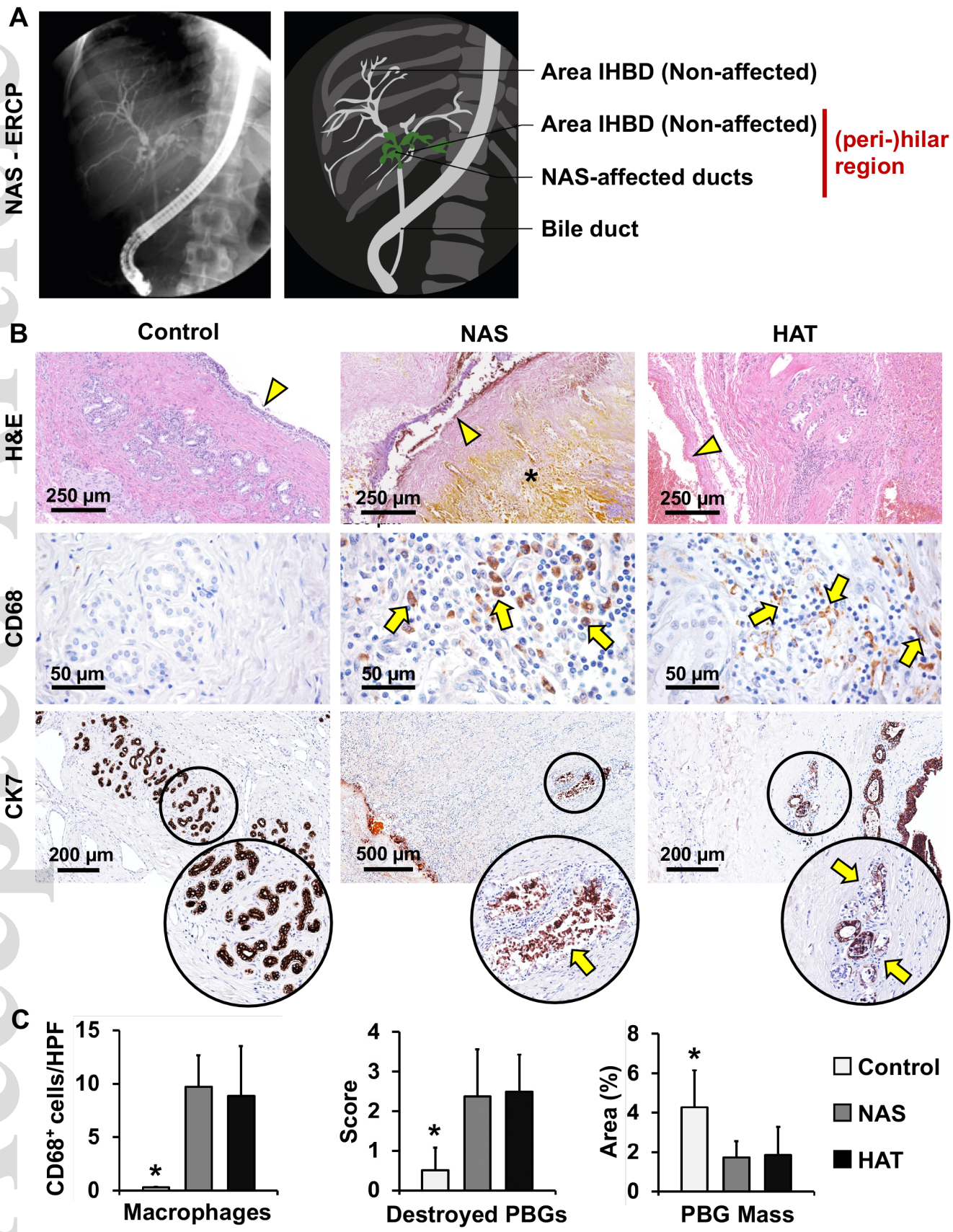

hep_32166_f1.tif

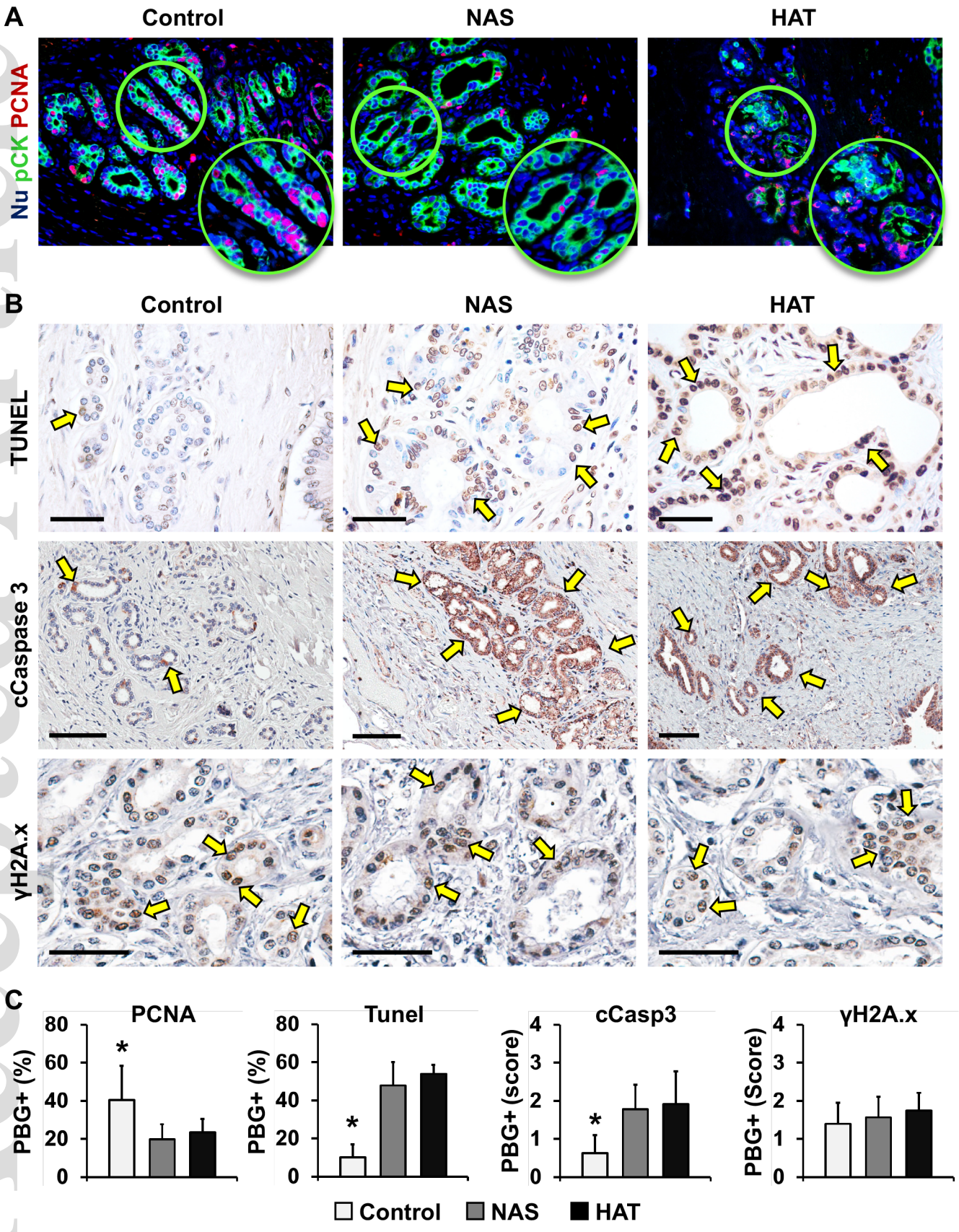

hep_32166_f2.tif

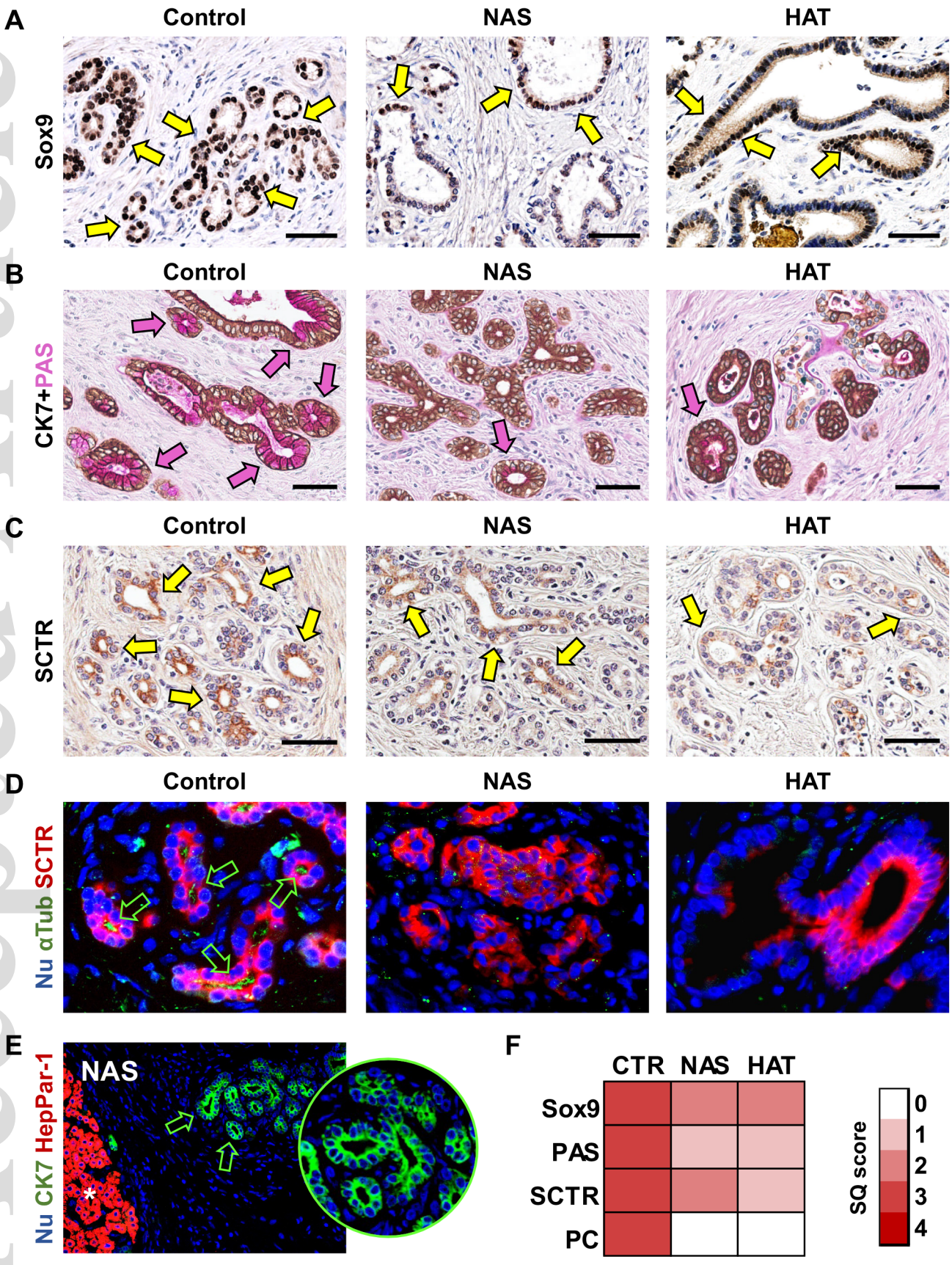

hep_32166_f3.tif

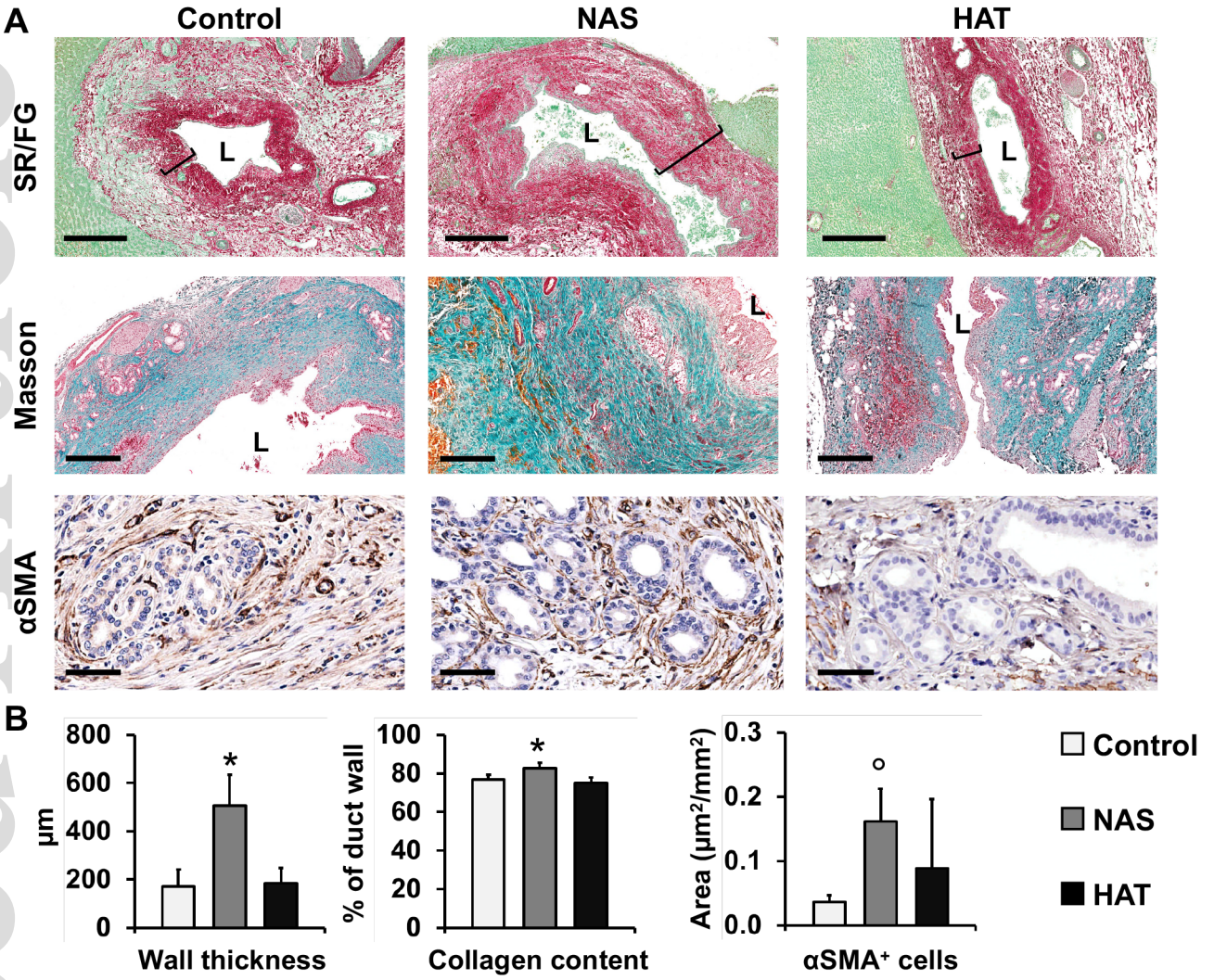

hep_32166_f4.tif

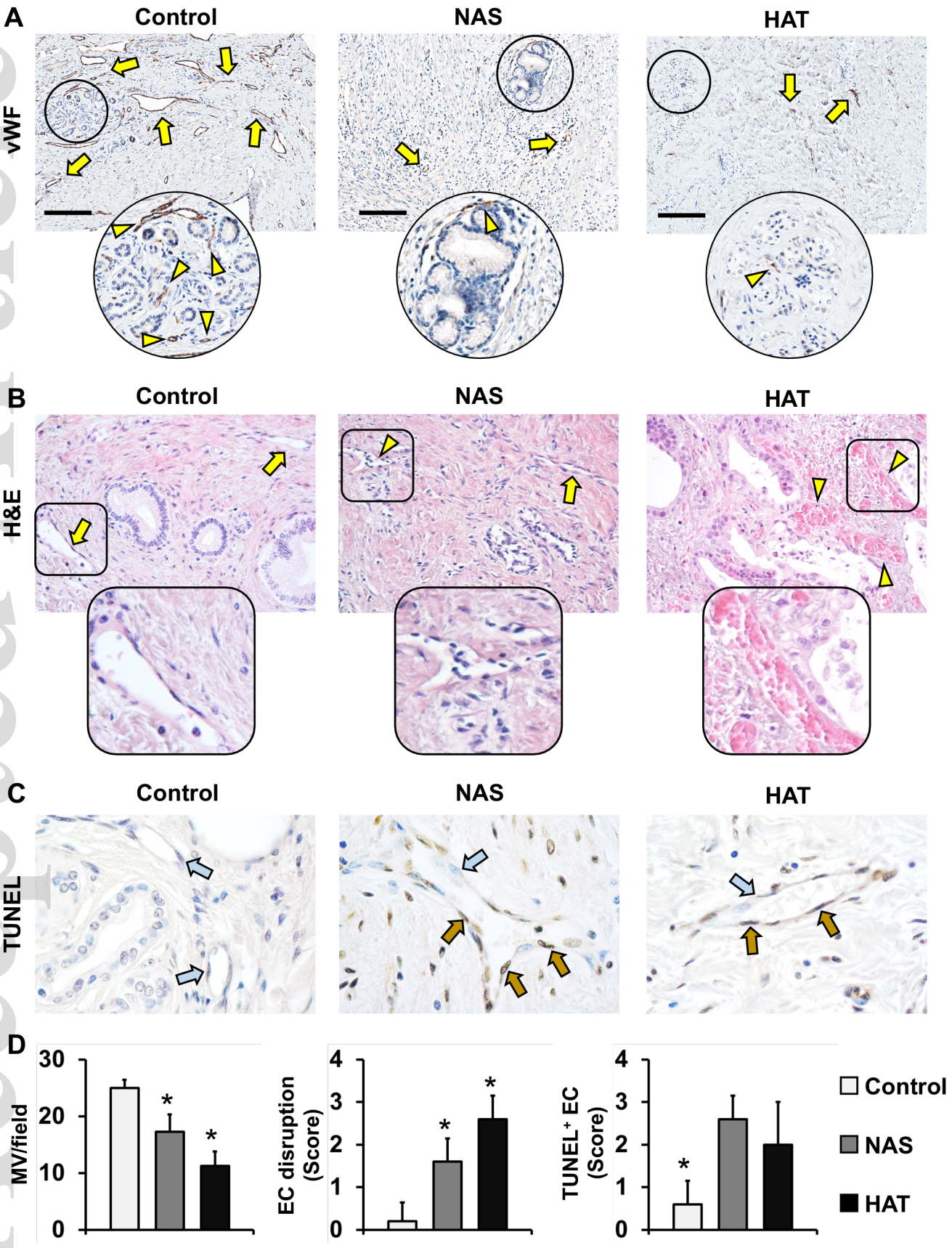

hep_32166_f5.tif

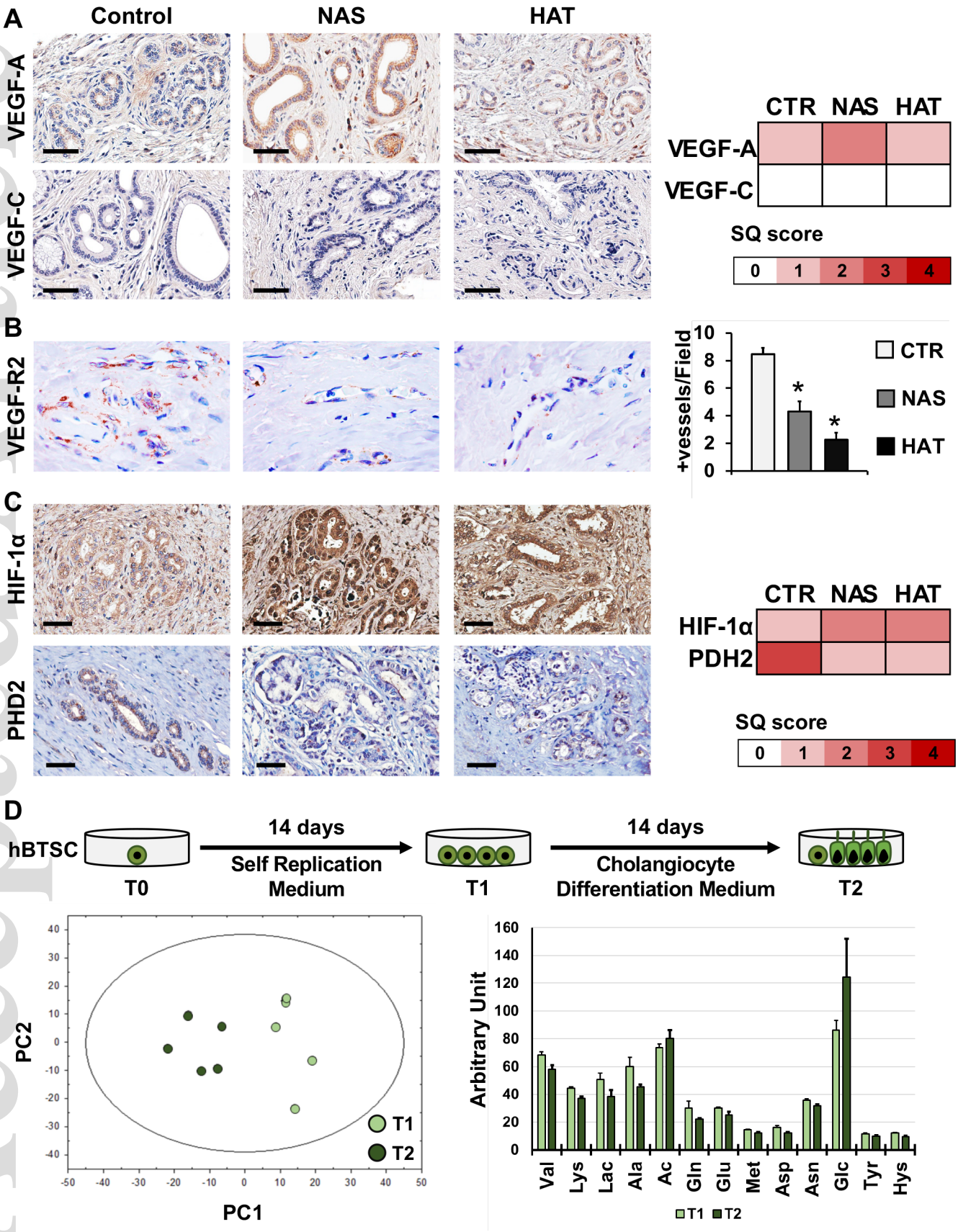

hep_32166_f6.tif